Journal of Computational Physics 231 (2012) 7504–7517

Contents lists available at SciVerse ScienceDirect

Journal of Computational Physics

journal homepage: www.elsevier.com/locate/jcp

Self-adjusting, positivity preserving high order schemes for hydrodynamics and magnetohydrodynamics

Dinshaw S. Balsara *

Physics Department, Univ. of Notre Dame, 225 Nieuwland Science Hall, Notre Dame, IN 46556, United States

ARTICLE INFO

Article history:
Received 24 October 2010
Received in revised form 18 January 2012
Accepted 20 January 2012
Available online 1 February 2012

Keywords:
Positivity
Higher order Godunov schemes
Reconstruction
ADER
WENO
Hydrodynamics
Magnetohydrodynamics

ABSTRACT

Several computational problems in science and engineering are stringent enough that maintaining positivity of density and pressure can become a problem. We build on the realization that positivity can be lost within a zone when reconstruction is carried out in the zone. We present a multidimensional, self-adjusting strategy for enforcing the positivity of density and pressure in hydrodynamic and magnetohydrodynamic (MHD) simulations. The MHD case has never been addressed before, and the hydrodynamic case has never been presented in quite the same way as done here. The method examines the local flow to identify regions with strong shocks. The permitted range of densities and pressures is also obtained at each zone by examining neighboring zones. The range is expanded if the solution is free of strong shocks in order to accommodate higher order non-oscillatory reconstructions. The density and pressure are then brought into the permitted range. The method has also been extended to MHD. It is very efficient and should extend to discontinuous Galerkin methods as well as flows on unstructured meshes.

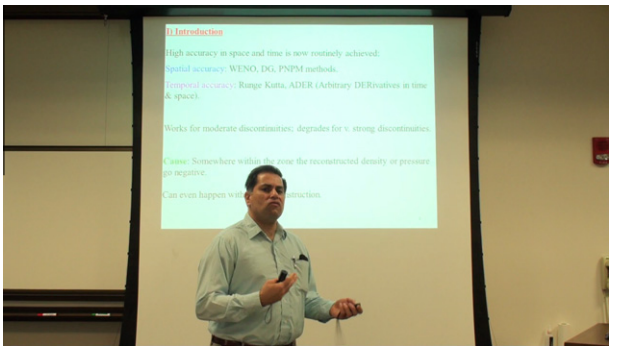

Video 1

The method presented here does not degrade the order of accuracy for smooth flows. Via a stringent test suite, we document that our method works well on structured meshes for all orders of accuracy up to four. When the same test problems are run without the positivity preserving methods, one sees a very clear degradation in the results, highlighting the value of the present method. The results are compelling because realistic simulation of several difficult astrophysical and space physics problems requires the use of parameters that are similar to the ones in our test problems.

* Tel.: +1 (574) 631 9639; fax: +1 (574) 631 5952.
E-mail address: dbalsara@nd.edu

0021-9991/$ - see front matter
http://dx.doi.org/10.1016/j.jcp.2012.01.032

In this work, weighted non-oscillatory reconstruction was applied to the conserved variables, i.e. we did not apply the reconstruction to the characteristic variables, which would have made the scheme more expensive. Yet, used in conjunction with the positivity preserving schemes presented here, the less expensive reconstruction works very well in two and three dimensions. The positivity preserving methods are easy to implement and inexpensive; they only increase the cost of reconstruction by a very small fraction. All these facts suggest that a self-adjusting positivity preserving algorithm is almost as important as non-linear hybridization in the design of robust, higher-order schemes.

1. Introduction

Hyperbolic systems of conservation laws play an important role in several areas of science and engineering. Excellent new methods have been designed for their accurate solution. Spatial accuracies that go beyond second order can be delivered by weighted essentially non-oscillatory schemes (WENO) [25,23,5,17,7,9], or by discontinuous Galerkin methods (DG) [13,14,38,39]. Higher order time accuracy has also become available via strong stability preserving Runge–Kutta methods [29–32], or via ADER (Arbitrary DERivatives in time and space) methods [35,33,18,7,9]. For smooth flow, or flow with discontinuities of moderate strength, such schemes perform very well, showing that the non-linear hybridization produced by the newer reconstruction techniques works well. For problems involving multiple, interacting shock waves in complex/turbulent flows, the methods can become temperamental performers. Reconstructing the solution in characteristic variables adds to the cost of the methods and might slightly ameliorate the problem, yet it usually does not solve the problem. This suggests that the problem indeed lies elsewhere. A careful examination of the computational zones where a spurious solution develops shows that somewhere within that zone the reconstructed profile has lost positivity of density or pressure. In other words, the reconstruction within the offending zone needs to be improved. A loss of density or pressure positivity renders the Euler system non-convex, thereby provoking further problems in its numerical solution.

The problem is not restricted to higher order schemes. Even within the context of second order schemes, where the reconstruction is carried out with TVD limiters, it is possible to show that this phenomenon does occur. The TVD property only ensures that the density does not become negative at the centers of zone faces, where the one-dimensional Riemann problem is usually solved. However, schemes that use multidimensional wave models [16,24,1,2,8,10] do invoke the Riemann solver at zone edges or vertices. The TVD reconstruction becomes an inadequate foil in such situations. Note that the zone-averaged value does still retain positive density and pressure, even as positivity is lost at some locations in the reconstructed profile.

Methods to rectify the problem have been attempted. Colella and Woodward [15] introduced a flattener algorithm that compares the local divergence of the velocity to the local sound speed and identifies regions where there are strong shocks. Similar flatteners have been devised for magnetohydrodynamics (MHD) [7]. When a local flow profile with some level of stringency is detected by the flattener, the variation in the reconstructed solution within that zone is suitably reduced. Titarev and Toro [34] enforced positivity in their WENO scheme by restricting the variation of the density and pressure in the reconstructed profile to lie within some fraction of the mean density and pressure within a zone. But that fraction remained fixed and did not adapt to the stringency in the local flow.

Barth [12] and Barth and Frederickson [11] introduced a multidimensional, self-adjusting strategy by realizing that for piecewise linear variations, the extrema in the reconstructed profile always occur at the vertices of a zone. By visiting the neighboring zones that have connectivity with a zone of interest, they were able to identify minimum and maximum values for all the flow variables that should bound the reconstructed profile within the zone of interest. The piecewise linear profile can then be reduced to lie within that range. At an operational level, this is accomplished by reducing the linear variation within a zone till the values at the vertices come within the range provided by the neighbors. Balsara [6] showed that this method extends seamlessly to second order accurate MHD algorithms. Some attempt to build in the logic of the flatteners, so as to extend the permissible range in Barth's method, would indeed make it suitable for providing a correction to essentially non-oscillatory limiting procedures. The first goal of this paper is to show how this is done.

Building on the work of Perthame and Shu [27], Zhang and Shu [40] have recently provided a method that also relies on restricting the variation of the reconstructed profile within a zone so as to restore positivity to the density and pressure variables. (Also see the work of Waagan [37].) They realized that the density and pressure only needs to be evaluated at a favorable set of nodal points within a zone. At those points they require that the density and pressure stay above certain absolute values for those variables. This is again accomplished by reducing the variation of the reconstructed profile within a zone. Their method works in practice, the only two deficiencies being that: (a) it is not self-adjusting and (b) it does not extend to other useful systems like MHD. The second goal of this paper is to provide a self-adjusting limiting strategy that permits the reconstructed profile to develop non-oscillatory extrema. The third goal is to show how all of the above-mentioned positivity preserving ideas extend to MHD, since the extension is non-trivial. The end result is a multidimensional, self-adjusting strategy for enforcing density and pressure positivity which also incorporates the guidance provided by the flatteners. The present strategy is extremely easy and inexpensive to implement as a small additional step in the reconstruction procedure for a higher order scheme. This is especially so for structured meshes where Balsara et al.

[9] have presented extremely inexpensive methods for obtaining the nodal values from the modal values within a zone for orders of accuracy up to four.

It was found during the course of this work that very inexpensive reconstruction strategies can be used even at high orders, as long as a self-adjusting positivity criterion is correctly applied. For that reason, the present paper seeks to elevate positivity to be a first ranked concept in the numerical solution of hyperbolic conservation laws, alongside with non-linear hybridization. In Section 2 we describe the method. In Section 3 we present results. Conclusions are presented in Section 4.

2. Self-adjusting positivity enforcing method for Euler and MHD flow

We describe the method on a two dimensional structured mesh, though it extends naturally to three dimensions and it could also extend naturally to unstructured meshes. Most of the examples presented in the next section are indeed three-dimensional. Let ρ and P be the density and pressure, let $\mathbf{v}$ be the velocity vector and let $\mathbf{B}$ be the magnetic field vector. Let γ be the ratio of specific heats. Let $\mathbf{m} \equiv \rho\mathbf{v}$ denote the momentum density and ε the energy density. For Euler flow we can write $\varepsilon = P/(\gamma - 1) + \rho\mathbf{v}^2/2$. For MHD flow we can write $\varepsilon = P/(\gamma - 1) + \rho\mathbf{v}^2/2 + \mathbf{B}^2/(8\pi)$. It helps to split the remainder of this section into three sub-sections. The first sub-section deals with Euler flow, the second sub-section deals with MHD flow and the third sub-section provides implementation related details and a pointwise recapitulation of the method.

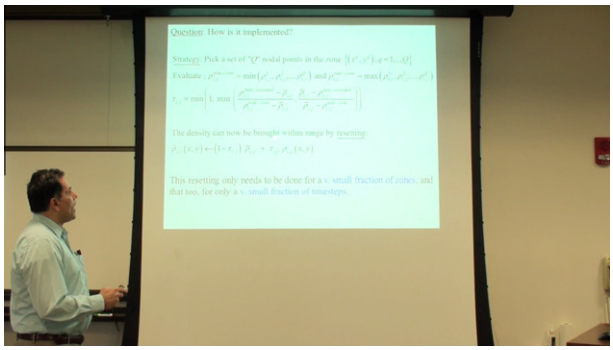

Video 2

2.1. Self-adjusting positivity enforcing method for Euler flow

We first need to define a flattener function that can identify regions of strong shocks within our computational domain. The method, therefore, begins by obtaining the divergence of the velocity, $(\nabla \cdot \mathbf{v})_{i,j}$, and the sound speed, $c_{s;i,j} \equiv \sqrt{\gamma P_{i,j}/\rho_{i,j}}$, within a zone (i,j) as shown in Fig. 1. For example, on a Cartesian mesh with zone sizes Δx and Δy,we can set $(\nabla \cdot \mathbf{v})_{i,j} = (v_{x;i+1,j} - v_{x;i-1,j})/\Delta x + (v_{y;i,j+1} - v_{y;i,j-1})/\Delta y$. To identify a shock, the undivided divergence of the velocity within a zone has to be compared with the minimum of the sound speed in the zone (i,j) and all its immediate neighbors. (The undivided divergence of the velocity can be defined within a zone by $(\nabla \cdot \mathbf{v})_{i,j}\min(\Delta x, \Delta y)$.) Thus we need the minimum sound speed from all the neighbors, see Fig. 1. It is defined by

$$c_{s;i,j}^{\min-nbr} = \min\left(c_{s;i-1,j-1}, c_{s;i-1,j}, c_{s;i-1,j+1}, c_{s;i,j-1}, c_{s;i,j}, c_{s;i,j+1}, c_{s;i+1,j-1}, c_{s;i+1,j}, c_{s;i+1,j+1},\right) \tag{1}$$

In each zone, which is assumed to have an extent Δx, we define the flattener as

$$\eta_{i,j} = \min\left[1, \max\left[0, -\left(\Delta x(\nabla \cdot \mathbf{v})_{i,j} + \kappa_1 c_{s;i,j}^{\min-nbr}\right) \Big/ \left(\kappa_1 c_{s;i,j}^{\min-nbr}\right)\right]\right] \tag{2}$$

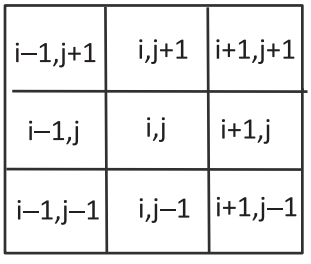

Fig. 1. showing the zones that are to be used on a two dimensional mesh to obtain the local maximum and minimum of a variable.

While there is some flexibility in the value of κ_1,here we take $\kappa_1 = 0.4$. Numerical experimentation has shown this value to work well at several orders and for a large range of problems. Please note that $(\nabla \cdot \mathbf{v})_{i,j}$ is obtained by finite differencing the zone averages and is not obtained from the reconstructed velocities. Notice from the structure of the above equation that when the flow develops rarefactions, i.e. $(\nabla \cdot \mathbf{v})_{i,j} \geqslant 0$, the reconstruction is left completely untouched by the flattener. For compressive motions of modest strength, i.e. when $-\kappa_1 c_{s:i,j}^{\min-nbr} < \Delta x(\nabla \cdot \mathbf{v})_{i,j} < 0$, the flattener also leaves the reconstruction untouched. We, therefore, see that $\eta_{i,j} = 0$ when the flow is smooth and it goes to $\eta_{i,j} = 1$ in a continuous fashion when strong shocks are present. It is possible to improve on the previous flattener. Zones that are about to be run over by a shock but have not yet entered the shock would also be stabilized if they were to experience some flattening. We identify such situations by looking at the pressure variation. We describe the method for the x-direction as

$$\begin{aligned} &\text{if } ((\eta_{i,j} > 0) \text{ and } (\eta_{i+1,j} = 0) \text{ and } (P_{i,j} > P_{i+1,j})) \text{ then } \eta_{i+1,j} = \eta_{i,j} \\ &\text{if } ((\eta_{i,j} > 0) \text{ and } (\eta_{i-1,j} = 0) \text{ and } (P_{i,j} > P_{i-1,j})) \text{ then } \eta_{i-1,j} = \eta_{i,j} \end{aligned} \tag{3}$$

Please note that Eq. (2) is applied first to the entire mesh in order to identify zones that are already inside a shock. Eq. (3) is applied subsequently in order to identify zones that are about to be run over by a shock. It is trivial to extend the above equation to the y-direction. For multidimensional problems, the above strategy can be applied to each of the principal directions of the mesh.

We now wish to obtain the minimum and maximum values of the density and pressure variables from the neighboring zones. For Fig. 1, we can do this for the density variable by setting

$$\begin{aligned} \rho_{i,j}^{\min-nbr} &= \min\left(\bar{\rho}_{i-1,j-1}, \bar{\rho}_{i-1,j}, \bar{\rho}_{i-1,j+1}, \bar{\rho}_{i,j-1}, \bar{\rho}_{i,j}, \bar{\rho}_{i,j+1}, \bar{\rho}_{i+1,j-1}, \bar{\rho}_{i+1,j}, \bar{\rho}_{i+1,j+1},\right) \\ \rho_{i,j}^{\max-nbr} &= \max\left(\bar{\rho}_{i-1,j-1}, \bar{\rho}_{i-1,j}, \bar{\rho}_{i-1,j+1}, \bar{\rho}_{i,j-1}, \bar{\rho}_{i,j}, \bar{\rho}_{i,j+1}, \bar{\rho}_{i+1,j-1}, \bar{\rho}_{i+1,j}, \bar{\rho}_{i+1,j+1},\right) \end{aligned} \tag{4}$$

where the overbars indicate zone-averaged values. Barth's limiting strategy, which is better suited for TVD schemes, would have demanded that $\rho_{i,j}^{\min-nbr} \leqslant \rho_{i,j}(x,y) \leqslant \rho_{i,j}^{\max-nbr}$ where $\rho_{i,j}(x,y)$ is the reconstructed density in the zone of interest. Similar expressions should be obtained for the pressure.

To accommodate non-oscillatory reconstruction schemes, we need to extend the range $\left[\rho_{i,j}^{\min-nbr}, \rho_{i,j}^{\max-nbr}\right]$ in a solution-dependent way. Using the flattener variable, this is done as:

$$\rho_{i,j}^{\min-extended} = \rho_{i,j}^{\min-nbr}(1 - \kappa_2 + \kappa_2\eta_{i,j}); \quad \rho_{i,j}^{\max-extended} = \rho_{i,j}^{\max-nbr}(1 + \kappa_2 - \kappa_2\eta_{i,j}) \tag{5}$$

While there is some flexibility in the value of κ_2, for this work we took $\kappa_2 = 0.4$. Numerical experimentation has shown this value to work well at several orders and for a large range of problems. To understand the reasoning behind Eq. (5), please realize that it does extend the range of permitted densities to $\left[(1-\kappa_2)\rho_{i,j}^{\min-nbr}, (1+\kappa_2)\rho_{i,j}^{\max-nbr}\right]$ in regions of smooth flow. If strong shocks are present in the vicinity of the zone of interest, the range of permitted densities is smoothly reduced to $\left[\rho_{i,j}^{\min-nbr}, \rho_{i,j}^{\max-nbr}\right]$ as the strength of the shocks become progressively larger. We can do similarly for the pressures. As a result, within each zone (i,j) we obtain a range of densities $\left[\rho_{i,j}^{\min-extended}, \rho_{i,j}^{\max-extended}\right]$ and demand that $\rho_{i,j}^{\min-extended} \leqslant \rho_{i,j}(x,y) \leqslant \rho_{i,j}^{\max-extended}$. Similarly, we obtain a range of pressures $\left[P_{i,j}^{\min-extended}, P_{i,j}^{\max-extended}\right]$ and demand that $P_{i,j}^{\min-extended} \leqslant P_{i,j}(x,y) \leqslant P_{i,j}^{\max-extended}$. In practice, it might be valuable to also provide absolute floor values for $\rho_{i,j}^{\min-extended}$ and $P_{i,j}^{\min-extended}$.

Notice from the previous two paragraphs that the density is a conserved variable and the zone-averaged density is already contained within the range $\left[\rho_{i,j}^{\min-extended}, \rho_{i,j}^{\max-extended}\right]$ by construction. Thus bringing the reconstructed density within the range simply requires us to reduce the spatially varying part of the density. The pressure, on the other hand, is a derived variable. While the zone-averaged pressure still lies within the range $\left[P_{i,j}^{\min-extended}, P_{i,j}^{\max-extended}\right]$, bringing the reconstructed pressure within this range is harder, especially since the reconstruction is almost always expressed in terms of the conserved variables. The next insight comes from Zhang and Shu [40] who presented an implementable strategy for doing this. For any conserved variable, say for instance the density in the zone (i,j), we can write

$$\widetilde{\rho}_{i,j}(x,y) = (1-\tau)\bar{\rho}_{i,j} + \tau\rho_{i,j}(x,y) \tag{6}$$

Here $\rho_{i,j}(x,y)$ is the original reconstructed profile in the zone of interest, $\bar{\rho}_{i,j}$ is the zone-averaged density and $\tau \in [0,1]$. Please do not confuse "τ" with the time variable. In this section it will refer exclusively to a parameter we use to restore positivity. When $\tau = 1$, the corrected profile $\widetilde{\rho}_{i,j}(x,y)$ is exactly equal to the original reconstructed profile $\rho_{i,j}(x,y)$. Thus if the entire reconstructed density lies within the desired range then such a situation is equivalent to setting $\tau = 1$ within that zone. If the reconstructed profile lies outside the range, one can always bring the corrected profile $\widetilde{\rho}_{i,j}(x,y)$ within the range by finding some $\tau < 1$ which accomplishes this. For $\tau = 0$, this is always satisfied, ensuring that any conserved variable can be brought within the desired range by progressively reducing the value of "τ" from unity till the variable is within the range.

The implementable strategy, which draws on Sanders [28], Barth [12] and Zhang and Shu [40], consists of having a set of "Q" nodal points $\{(x^q, y^q); q = 1, \ldots, Q\}$ within each zone and evaluating the entire vector of conserved variables at those points. The index "q" tags the nodal points within each zone. It is worth pointing out that the present strategy requires a

judicious choice of nodal points in order to work well. In Subsection 2.3 we will explicit the nodal points at various orders for a structured mesh. Thus we have $\rho^q_{i,j} \equiv \rho_{i,j}(x^q, y^q)$ and we can also use them to find $\rho^{\min-zone}_{i,j} = \min\left(\rho^1_{i,j}, \rho^2_{i,j}, \ldots, \rho^Q_{i,j}\right)$ and $\rho^{\max-zone}_{i,j} = \max\left(\rho^1_{i,j}, \rho^2_{i,j}, \ldots, \rho^Q_{i,j}\right)$. As shown by Barth [12], within each zone (i,j) we can obtain a variable

$$\tau_{i,j} = \min\left(1, \min\left(\frac{\rho^{\max-extended}_{i,j} - \bar{\rho}_{i,j}}{\rho^{\max-zone}_{i,j} - \bar{\rho}_{i,j}}, \frac{\bar{\rho}_{i,j} - \rho^{\min-extended}_{i,j}}{\bar{\rho}_{i,j} - \rho^{\min-zone}_{i,j}}\right)\right) \tag{7}$$

Then the corrected profile for the density, which lies within the desired solution-dependent range and has sufficient leeway to be a non-oscillatory reconstruction, is given by

$$\widetilde{\rho}_{i,j}(x,y) = (1-\tau_{i,j})\bar{\rho}_{i,j} + \tau_{i,j}\rho_{i,j}(x,y) \tag{8}$$

For most practical calculations, this correction will only be invoked in an extremely small fraction of zones and, that too, for a very small fraction of the total number of time steps. In practice, the physical velocity should not change when the density profile is corrected. Since the momentum density scales as the density, when the variation in the density is reduced, it also helps to reduce the variation in the momentum density by the same amount. Similarly, the variation in the total energy density should also be reduced by the same amount.

The previous paragraph has shown how the density is brought within the desired range. We now describe the process of bringing the pressure within the desired range for Euler flow. The positivity for the pressure variable is enforced after the positivity fixes for the density variable have been incorporated, as described in the previous paragraph. The philosophy applied here is quite similar to the one used for the density. The only difference is that the pressure is a derived variable. Thus we write

$$\begin{aligned} &\widetilde{\rho}_{i,j}(x,y) = (1-\tau)\bar{\rho}_{i,j} + \tau\rho_{i,j}(x,y); \quad \widetilde{\mathbf{m}}_{i,j}(x,y) = (1-\tau)\bar{\mathbf{m}}_{i,j} + \tau\mathbf{m}_{i,j}(x,y); \\ &\widetilde{\varepsilon}_{i,j}(x,y) = (1-\tau)\bar{\varepsilon}_{i,j} + \tau\varepsilon_{i,j}(x,y) \end{aligned} \tag{9}$$

As before we have $\tau \in [0,1]$, and we observe that with $\tau = 0$ the pressure is guaranteed to be within the desired range. Recall that the zone-averaged variables do have positive pressure. Working with the previously defined nodal points, we can define $\rho^q_{i,j} \equiv \rho_{i,j}(x^q, y^q), \mathbf{m}^q_{i,j} \equiv \mathbf{m}_{i,j}(x^q, y^q)$ and $\varepsilon^q_{i,j} \equiv \varepsilon_{i,j}(x^q, y^q)$. We can then define the pressure at each nodal point by

$$P^q_{i,j} = (\gamma-1)\left(\varepsilon^q_{i,j} - \frac{\left(\mathbf{m}^q_{i,j}\right)^2}{2\rho^q_{i,j}}\right) \tag{10}$$

If $P^q_{i,j}$ lies within the desired range of pressures, we set a nodal variable $\tau^q_{i,j} = 1$. If $P^q_{i,j}$ is not within the desired range, we wish to find a nodal variable $\tau^q_{i,j} < 1$ which brings it within the desired range. We illustrate the case where the $P^{\min-extended}_{i,j}$ bound is violated by the qth nodal point. The variable $\tau^q_{i,j} < 1$ which brings that nodal pressure back within the desired range is given by solving

$$(\gamma-1)\left\{\left[\left(1-\tau^q_{i,j}\right)\bar{\varepsilon}_{i,j} + \tau^q_{i,j}\varepsilon^q_{i,j}\right] - \frac{1}{2}\frac{\left[\left(1-\tau^q_{i,j}\right)\bar{\mathbf{m}}_{i,j} + \tau^q_{i,j}\mathbf{m}^q_{i,j}\right]^2}{\left[\left(1-\tau^q_{i,j}\right)\bar{\rho}_{i,j} + \tau^q_{i,j}\rho^q_{i,j}\right]}\right\} = P^{\min-extended}_{i,j} \tag{11}$$

The above equation is easy to solve for $\tau^q_{i,j}$ because it is actually a quadratic, a fact made apparent by writing it explicitly as

$$\begin{aligned} &\left(\tau^q_{i,j}\right)^2\left[2\left(\rho^q_{i,j} - \bar{\rho}_{i,j}\right)\left(\varepsilon^q_{i,j} - \bar{\varepsilon}_{i,j}\right) - \left(\mathbf{m}^q_{i,j} - \bar{\mathbf{m}}_{i,j}\right)^2\right] \\ &+ \left(\tau^q_{i,j}\right)\left[2\bar{\rho}_{i,j}\left(\varepsilon^q_{i,j} - \bar{\varepsilon}_{i,j}\right) + 2\bar{\varepsilon}_{i,j}\left(\rho^q_{i,j} - \bar{\rho}_{i,j}\right) - 2\left(\mathbf{m}^q_{i,j} - \bar{\mathbf{m}}_{i,j}\right)\cdot\bar{\mathbf{m}}_{i,j} - 2\mathrm{e}^{\min-extended}_{i,j}\left(\rho^q_{i,j} - \bar{\rho}_{i,j}\right)\right] \\ &+ \left[2\bar{\rho}_{i,j}\bar{\varepsilon}_{i,j} - (\bar{\mathbf{m}}_{i,j})^2 - 2\mathrm{e}^{\min-extended}_{i,j}\bar{\rho}_{i,j}\right] = 0 \\ &\qquad\qquad \text{with } \mathrm{e}^{\min-extended}_{i,j} \equiv P^{\min-extended}_{i,j}/(\gamma-1) \end{aligned} \tag{12}$$

The above step should be done for all the defective nodes within a zone. As before, we expect that only a very small fraction of zones in a practical computation will need this pressure positivity fix. We can then find $\tau_{i,j} = \min\left(\tau^1_{i,j}, \tau^2_{i,j}, \ldots, \tau^Q_{i,j}\right)$. As before, $\tau_{i,j}$ can now be used to shrink the spatially varying part of all the conserved variables in zone (i,j); i.e. as shown in Eq. (9). Indeed note from the above two equations that one has to shrink the spatial variation of *all* the conserved variables in order to bring *all* the nodal pressures within the desired range. This completes our description of the positivity preserving scheme for Euler flow.

2.2. Self-adjusting positivity enforcing method for MHD flow

We now turn our attention to MHD. The enforcement of density positivity is exactly similar to the strategy described in the previous sub-section. The only difference is that we now redefine $c_{s;i,j} \equiv \sqrt{\left(\gamma P_{i,j} + (\bar{B}_{i,j})^2/4\pi\right)/\bar{\rho}_{i,j}}$. I.e. $c_{s;i,j}$ is redefined to be a maximal magnetosonic speed in the local flow. We do not repeat the details for enforcing density positivity, since they are the same as the Euler case. The remaining part of this sub-section describes the enforcement of pressure positivity.

In a divergence-free scheme for MHD, the components of the magnetic field are specified at zone boundaries. All the moments of the magnetic field, including the zeroth moments, have to be retrieved *within* a zone. When dealing with the magnetic field, it turns out that certain modes of the magnetic field can be reconstructed whereas other modes are required to satisfy a consistency condition at zone boundaries, Balsara et al. [9]. For example, in Section 3 of their paper, Balsara et al. [9] show that when reconstructing the x-magnetic field within a zone at second order, its piecewise linear variation in the x-direction has to satisfy a consistency condition with the magnetic field at the x-faces. Likewise, they showed that when reconstructing the x-magnetic field within a zone at third order, its piecewise linear and parabolic variations in the x-direction have to satisfy a consistency condition with the magnetic field at the x-faces. The other moments can be set by any order-preserving, non-linearly hybridized reconstruction method. For that reason, in situations where the variation in the magnetic field has to be reduced for the sake of positivity, we suggest reducing the variation in just the modes that may be freely changed, i.e. the modes that can be reconstructed without regard to consistency. Thus let $\bar{\mathbf{B}}^q_{i,j}$ be the part of the magnetic field that is needed by the consistency condition at the nodal point (x^q,y^q) in the zone (i,j). This part includes the constant parts (zeroth moments) of the magnetic field components, as well as the small number of spatially-varying moments that are required for consistency. These small number of spatially varying moments make $\bar{B}^q_{i,j}$ spatially varying within the zone (i,j). Let the remaining part of the magnetic field at the nodal point (x^q,y^q) in the zone (i,j) be denoted by $\mathbf{B}^q_{i,j}$. This part does not include the constant parts of the magnetic field. The permitted variation in the magnetic field at a nodal point can then by written as

$$\bar{\mathbf{B}}^q_{i,j} + \tau^q_{i,j}\mathbf{B}^q_{i,j} \tag{13}$$

As before, the variation in the magnetic field is modulated by the nodal variable $\tau^q_{i,j}$. It is this variation that can be reduced when positivity is enforced.

In order to describe how pressure positivity is enforced, we again provide the example where the $P^{\min-extended}_{i,j}$ bound is violated at the qth nodal point. The variable $\tau^q_{i,j} < 1$ which brings that nodal pressure back within the desired range is given by solving

$$(\gamma-1)\left\{\left[\left(1-\tau^q_{i,j}\right)\bar{\varepsilon}_{i,j}+\tau^q_{i,j}\varepsilon^q_{i,j}\right]-\frac{1}{2}\frac{\left[\left(1-\tau^q_{i,j}\right)\bar{\mathbf{m}}_{i,j}+\tau^q_{i,j}\mathbf{m}^q_{i,j}\right]^2}{\left[\left(1-\tau^q_{i,j}\right)\bar{\rho}_{i,j}+\tau^q_{i,j}\rho^q_{i,j}\right]}-\frac{1}{8\pi}\left[\bar{\mathbf{B}}^q_{i,j}+\tau^q_{i,j}\mathbf{B}^q_{i,j}\right]^2\right\} = P^{\min-extended}_{i,j} \tag{14}$$

We make the simplifications $\bar{\mathbf{B}}^q_{i,j} \to \bar{\mathbf{B}}^q_{i,j}/\sqrt{4\pi}$ and $\mathbf{B}^q_{i,j} \to \mathbf{B}^q_{i,j}/\sqrt{4\pi}$. The above equation is quite easy to solve for $\tau^q_{i,j}$ because it is actually a cubic, a fact made apparent by writing it explicitly as

$$\begin{aligned}
&\left(\tau^q_{i,j}\right)^3\left[-\left(\rho^q_{i,j}-\bar{\rho}_{i,j}\right)\left(\mathbf{B}^q_{i,j}\right)^2\right]\\
&+\left(\tau^q_{i,j}\right)^2\left[2\left(\rho^q_{i,j}-\bar{\rho}_{i,j}\right)\left(\varepsilon^q_{i,j}-\bar{\varepsilon}_{i,j}\right)-\left(\mathbf{m}^q_{i,j}-\bar{\mathbf{m}}_{i,j}\right)^2-\bar{\rho}_{i,j}\left(\mathbf{B}^q_{i,j}\right)^2-2\left(\rho^q_{i,j}-\bar{\rho}_{i,j}\right)\mathbf{B}^q_{i,j}\cdot\bar{B}^q_{i,j}\right]\\
&+\left(\tau^q_{i,j}\right)\begin{bmatrix}2\bar{\rho}_{i,j}\left(\varepsilon^q_{i,j}-\bar{\varepsilon}_{i,j}\right)+2\bar{\varepsilon}_{i,j}\left(\rho^q_{i,j}-\bar{\rho}_{i,j}\right)-2\left(\mathbf{m}^q_{i,j}-\bar{\mathbf{m}}_{i,j}\right)\cdot\bar{\mathbf{m}}_{i,j}-2\bar{\rho}_{i,j}\mathbf{B}^q_{i,j}\cdot\bar{\mathbf{B}}^q_{i,j}\\ -\left(\rho^q_{i,j}-\bar{\rho}_{i,j}\right)\left(\bar{\mathbf{B}}^q_{i,j}\right)^2-2\mathrm{e}^{\min-extended}_{i,j}\left(\rho^q_{i,j}-\bar{\rho}_{i,j}\right)\end{bmatrix}\\
&+\left[2\bar{\rho}_{i,j}\bar{\varepsilon}_{i,j}-(\bar{\mathbf{m}}_{i,j})^2-\bar{\rho}_{i,j}\left(\bar{\mathbf{B}}^q_{i,j}\right)^2-2\mathrm{e}^{\min-extended}_{i,j}\bar{\rho}_{i,j}\right]=0\\
&\qquad\qquad\text{with } \mathrm{e}^{\min-extended}_{i,j} \equiv P^{\min-extended}_{i,j}/(\gamma-1)
\end{aligned} \tag{15}$$

Please note that the third square bracket in the above equation is not a matrix, but rather evaluates to a scalar value. The above cubic is easily iterated to convergence because we already know that $\tau^q_{i,j} \in [0,1]$, i.e. the bracketing of the root is known in advance. Thus a Newton method for its iterative solution can always be stabilized by bisection. The above cubic does not need to be solved to convergence; just reducing the error by a few (three to four) significant places is sufficient because the pressure positivity fix is just meant to bring the pressure variable back into the physical range. Best of all, the method converges fast and is only invoked in a very small fraction of the total zones in a computation. We have found a maximum of four iterations to be sufficient for all the simulations that we have ever run.

2.3. Implementation-related details and pointwise recapitulation of the method

The present method works well for Runge–Kutta and ADER time stepping. For a Runge–Kutta method, it should be applied to each stage after the reconstruction but before the call to the Riemann solver. For an ADER method, it should be applied after the reconstruction but before the predictor step.

In practice, only the lower bound of the pressure needs to be brought in line with the physics of the problem. Consequently, that is the only bound that we enforce on the pressure variable. The upper bound can also be enforced on the pressure variable if there seems to be a compelling need. But in all our applications we have not seen it. Both the lower and the upper bounds are imposed on the density though.

It is important to choose a good set of nodes. Zhang and Shu [40] suggest using a tensor product of Gauss–Lobatto points, but that would result in an excessive number of nodes in multiple dimensions. This would especially be true as the order is increased. A better choice would be to choose as many nodes as are needed to make a nodal to modal transcription. I.e. as shown in Balsara et al. [9], there are a small number of symmetrically placed nodes at each order which are sufficient to take a set of nodal fluxes and obtain their modal equivalents. To this minimal set of nodes, it helps to add a few more. For piecewise linear reconstruction, it is easy to see that the extrema of the variation within a zone occur at the vertices. Please note that the nodes that are used for positivity are purely spatial, they do not include the space–time nodes that are used in the ADER construction. Thus at second order and in three dimensions, we take the eight vertices of each zone as our minimal set of nodes. Since piecewise linear variation is always present in any reconstruction, it is always a good practice to include the vertices of each zone in any test of positivity. The nodal set presented in Balsara et al. [9] includes thirteen spatial nodes at third order. Since those nodes do not include the zone's vertices, we add them to the set of nodes, yielding a set of twenty-one spatial nodes in three dimensions at which the pressure positivity is enforced for a third order scheme. The nodal set presented in Balsara et al. [9] includes twenty-one spatial nodes at fourth order. Since that set of nodes includes the zone's vertices, the positivity at fourth order is also imposed on a set of twenty-one spatial nodes. At fifth and higher orders, similar sets of nodes may be found. Since we do not document schemes at fifth and higher orders in this paper, we do not document the choice of nodes for those schemes here. For most practical work in CFD, fourth order accuracy proves to be amply sufficient.

As shown by Einfeldt et al. [19], linearized Riemann solvers produce an unphysical loss of pressure positivity in regions with large rarefactions. While a fix-up is attempted in that paper for Euler flows, obtaining such a fix for other systems might prove to be very strenuous. For that reason, we retain an entropy formulation, as suggested in Balsara and Spicer [3]. It is never needed at shocks, where conservation is an issue. However, it helps in regions with strong rarefactions. In general, it is best to use positivity preserving Riemann solvers [36,20,26,37,8,10] when they are available.

The alert reader will have noticed that we do not directly limit the range of velocities; though it is implicitly limited by the pressure positivity. Similarly, for MHD, we do not explicitly limit the range of the magnetic fields, though it too is tacitly limited by the pressure positivity. For the test problems shown, we have not seen a need to directly limit the velocities or the magnetic fields. Yet, there are several situations where it might be desirable to do so, which we catalogue here. First, in the vicinity of extremely strong shocks, it may prove advantageous to limit the velocity range. Second, instead of reconstructing the moments through an inherently non-linear procedure like the WENO method used here, one may want to construct the moments via a less expensive method, like a least squares procedure. In that case, it is indeed meaningful to limit the range of velocities. Third, realize that a DG scheme evolves all the moments. In such a situation, the limiting only needs to be applied to troubled zones, and the flattener does a good job of identifying the troubled zones. Consequently, the only limiting that one might need for DG schemes might consist of bringing the velocity and magnetic field variation within acceptable ranges. (One would of course have to do the same for the density and pressure variations.) For these reasons, the appendix catalogues a procedure for bringing the velocity and magnetic fields within desired ranges.

The positivity preserving strategy is documented in pointwise form below:

(1) Apply Eqs. (1)–(3) to obtain the flattener in each zone.
(2) Apply Eqs. (4) and (5) in each zone to obtain $\rho_{i,j}^{\min-extended}$ and $\rho_{i,j}^{\max-extended}$. Do likewise for the pressure.
(3) For each of the nodes "q" within a zone, obtain $\rho_{i,j}^{q}$. Then use Eq. (7) to obtain $\tau_{i,j}$ only for the offending zones. Use this value of $\tau_{i,j}$ to reduce the variation of the conserved variables within just the problematic zones.
4) For the same nodal points as above, obtain $\rho_{i,j}^{q}$, $\mathbf{m}_{i,j}^{q}$ and $\varepsilon_{i,j}^{q}$. (For MHD, also obtain $\overline{\mathbf{B}}_{i,j}^{q}$ and $\mathbf{B}_{i,j}^{q}$.) Do this for all the zones.
5) Using Eq. (12) for Euler flow and Eq. (15) for MHD, obtain $\tau_{i,j}^{q}$ only for the offending nodes in the offending zones. Find $\tau_{i,j} = \min\left(\tau_{i,j}^{1}, \tau_{i,j}^{2}, \ldots, \tau_{i,j}^{Q},\right)$ and use it to reduce the variation of the conserved variables in just the problematic zones.

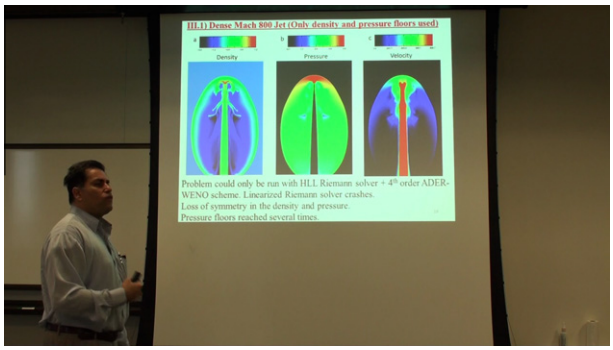

Video 3

3. Results

In Balsara et al. [7] we presented a suite of smooth test problems that were designed to demonstrate the order of accuracy of the ADER-WENO scheme. The test suite was run again using the positivity preserving scheme that is presented here. The accuracy of the ADER-WENO scheme, even at higher orders, stays unchanged when the present positivity scheme is added to the overall scheme. This shows us that for smooth Euler and MHD flows the method presented here does not damage accuracy.

For Euler flows, the positivity preserving scheme is only needed in very high Mach number situations where the kinetic energy density is much larger than the thermal energy density. For MHD flows, the positivity preserving scheme is needed in situations where the Mach number is very high or in situations where the magnetic energy density exceeds the thermal energy density by a very wide margin. The simulations presented here, therefore, focus on such extreme computational problems.

In the next three sub-sections we present three very stringent test problems for Euler and MHD flow. The first two hydrodynamical simulations pertain to a Mach 800 dense jet and an analogous light jet. The third MHD simulation pertains to a strong blast in a low-β plasma. All three simulations generate values that are very commonly found in astrophysical and space physics simulations. The proper operation of the positivity preserving schemes presented here, therefore, demonstrates their immense utility in high accuracy simulations in each of these two scientifically important areas. We also mention that second order TVD limiters will also produce pathological results if they are used on these problems without the methods developed here. Thus the pathologies do not arise at third and higher orders of accuracy but also plague second order schemes.

The interested reader may well ask whether one can supply a simple floor to the density and pressure when running these stringent problems? The rationale for this question stems from the realization that when the computation is likely to develop a pathology, providing a floor for the density and pressure is one possible fix-up that is easily implemented and often used. In most practical situations, the density and/or pressure in the simulation will hit that floor value during the course of such a computation. What happens to the simulation after that point is difficult to predict because the simulation has already reached a pathological state. The simulation may choose to tear itself apart, or it may choose to produce a density or pressure that is consistently unreliable. We decided to test this possibility by running the three above-mentioned simulations with the positivity enforcement mechanisms discussed here. We then ran them again without the positivity enforcement mechanisms, but by supplying a simple density floor of 1×10^{-12} and a pressure floor of 1×10^{-8} in the Riemann solver. Since wave propagation speeds are evaluated in any Riemann solver, this is the one place in the code where input densities and pressures must be positive. The timestep calculation is the other place in the code where positive densities and pressures must be supplied. All the simulations presented here are such that the Riemann solver will certainly receive negative values of the density or pressure, thereby triggering a code crash, if no floor values are supplied.

We found that one of the two hydrodynamical jet simulations simply cannot be run with a simple-minded density and pressure floor. In the problematical jet simulation, we found that the pressure floor is reached rather early for several timesteps. After that point, a density floor is also reached. Eventually, the timestep bottoms out and the simulation simply stops. Consequently, the result of supplying a simple density and pressure floor without the use of the proposed methods cannot be displayed for one our examples. In the MHD blast simulation, we indeed succeeded in running the simulation with the simple density and pressure floors, only to find that the pressure floor is reached at several locations in the simulation. This renders the simulation useless for scientific purposes. This result was also seen to occur when a second order TVD scheme was used. We, nevertheless, do display the final result. Our overall conclusion is that the positivity preserving methods presented here are vitally important in retaining physical consistency in several important astrophysical and space physics simulations.

3.1. 2D Mach 800 dense adiabatic jet

This problem is very much like the problem presented in Ha et al. [21] and Ha and Gardner [22]. It consists of a dense fluid slab jet in two dimensions propagating through a lighter ambient medium. It is patterned after galactic astrophysical jets which tend to be denser than their ambient medium and tend to have high Mach numbers. We take $\gamma = 1.4$ for the fluid. The jet density and pressure are given by $\rho_j = \gamma$ and $P_j = 1$ so that the sound speed in the jet is unity. The pressure in the ambient, matches that in the jet. The density of the ambient gas is given by $\rho_a = 0.1\gamma$; i.e. the jet density exceeds the ambient density by a factor of ten. The computational domain has 400×600 zones and is given by $[-0.5, 0.5] \times [0, 1.5]$. Because the density and pressure in the jet yield a sound speed of unity, the jet's velocity at the inlet is set to 800. The jet enters the center of the short dimension of the computational domain and has a width of 0.1. The other boundaries are outflow boundary conditions.

The problem was simulated with a fourth order accurate ADER-WENO scheme using a linearized Riemann solver. The use of a linearized Riemann solver, instead of an HLL Riemann solver, makes this problem more challenging. (We note parenthetically that Zhang and Shu [40] only used an LLF Riemann solver.) Zhang and Shu [40] claim that their method restricts the CFL number. However, the ADER method couples space and time more effectively. As a result, the present method works with sufficiently large CFL numbers. In this problem, a robust CFL number of 0.45 was used. The simulation was run to a time of 0.002 and the results from the final time are displayed.

Fig. 2a shows the log (base-10) color plot of the density. Fig. 2b shows the same for the pressure. Fig. 2c shows the magnitude of the velocity. We see that the densities and pressures are positive as expected. The methods developed in this paper

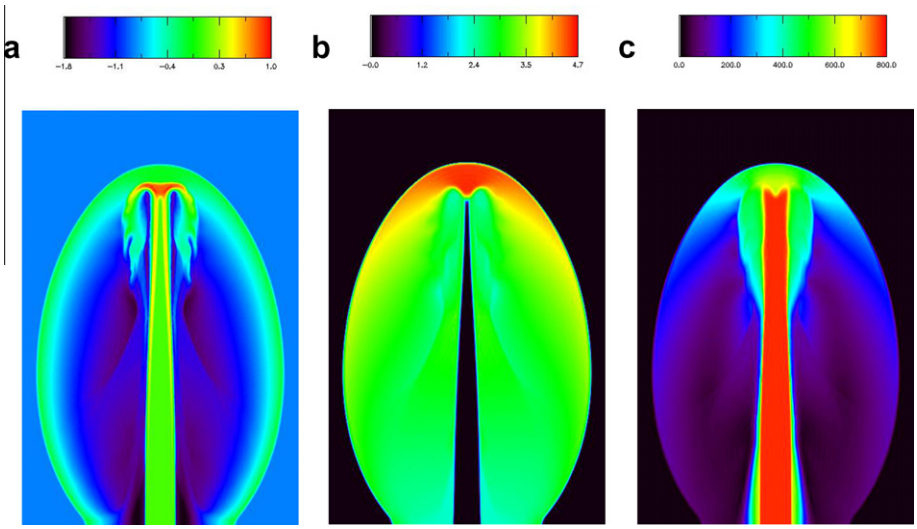

Fig. 2. a, b and c from the dense jet simulation, show the logarithmic density (base-10), logarithmic pressure (base-10) and magnitude of the velocity. The color bars show the logarithmic (base-10) values for the density and pressure and the magnitude of the velocity. The range for the density (not log density) is [0.0159, 10.8]. Similarly, the range for the pressure (not log pressure) is [0.981, 52583.4]. For the magnitude of the velocity, the range is [0, 800].

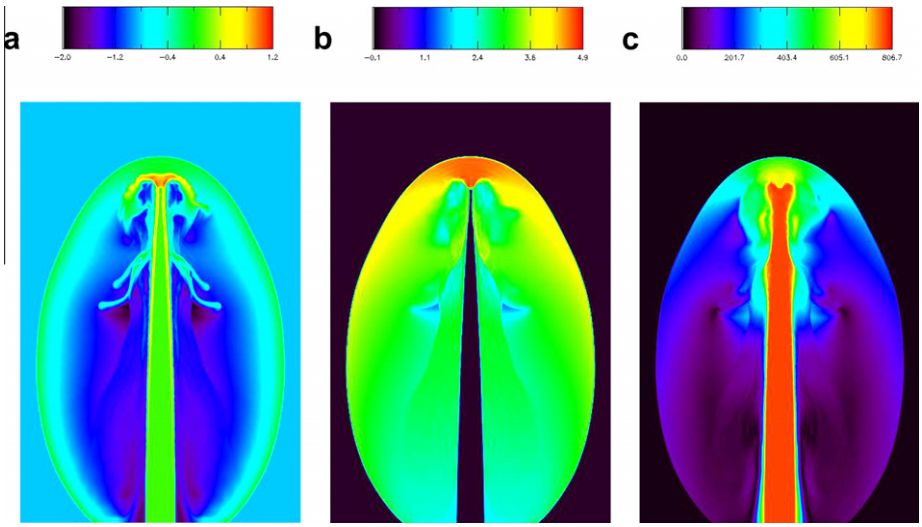

Fig. 3. a, b and c from the dense jet simulation, show the logarithmic density (base-10), logarithmic pressure (base-10) and magnitude of the velocity. In this simulation, the methods from this paper were not used. An HLL Riemann solver with floor values for the density and pressure was used instead. Notice the unphysical loss of symmetry in the density variable. The color bars show the logarithmic (base-10) values for the density and pressure and the magnitude of the velocity. The range for the density (not log density) is [0.0089, 16.37]. Similarly, the range for the pressure (not log pressure) is [0.808, 73651.7]. For the magnitude of the velocity, the range is [0, 800].

were applied to the simulation that is reported in Fig. 2. The fluid flows through the jet's channel till it shocks at the working surface. Observe the rise in the density and pressure at the working surface. The high pressure at the working surface deflects the jet fluid backwards will it forms a cocoon around the jet, as can be seen in the density variable.

This problem cannot be simulated with an unmodified second order TVD scheme and a linearized Riemann solver. Nor can it be simulated with higher order schemes when simple density and pressure floors are provided to a linearized Riemann solver. When an HLL Riemann solver is used along with density and pressure floors, the problem produces several intermediate timesteps with a pressure floor value, but it does run through to the final time. Fig. 3a, b and c show the log (base-10) color plot of the density, log (base-10) color plot of the pressure and the magnitude of the velocity when the problem is simulated without using the methods proposed in this paper. For the simulation reported in Fig. 3, a simple density and pressure floor, as described before, were supplied to an HLL Riemann solver which is used along with an unmodified fourth order ADER-WENO scheme. With such an algorithmic combination, the problem does run through. However, the density variable in Fig. 3a shows a dramatic and unphysical loss of symmetry which is especially visible close to the working surface of the jet. We realize, therefore, that even when a beneficial algorithmic combination is used with simple-minded density and pres-

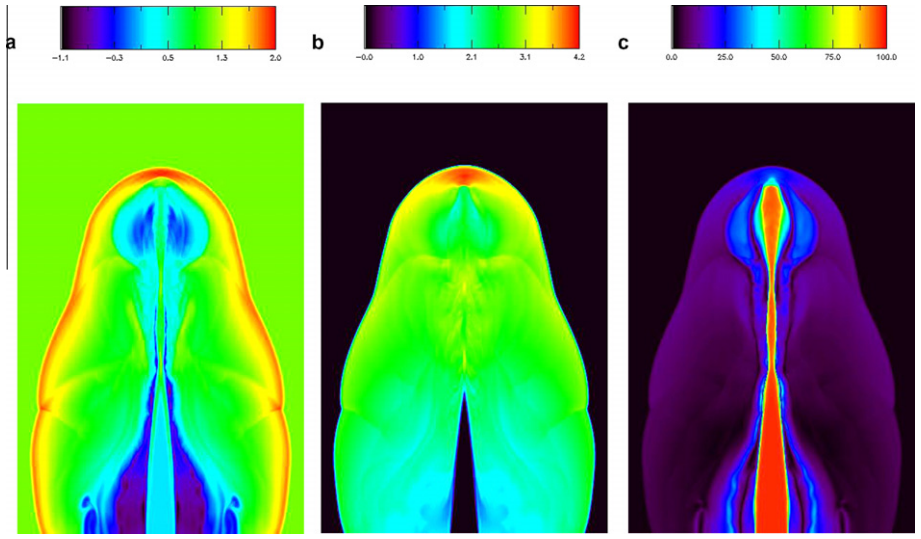

Fig. 4. a, b and c from the light jet simulation, show the logarithmic density (base-10), logarithmic pressure (base-10) and magnitude of the velocity. The color bars show the logarithmic (base-10) values for the density and pressure and the magnitude of the velocity. The range for the density (not log density) is [0.0809, 110.3]. Similarly, the range for the pressure (not log pressure) is [0.998, 14960.0]. For the magnitude of the velocity, the range is [0, 100].

sure floors, the simulation inevitably shows some noticeable pathology. A comparison of Figs. 2 and 3 shows the obvious advantages of the methods developed in this paper.

3.2. 2D Mach 100 light adiabatic jet

The set up for this problem is indeed very similar to that for the dense jet, the key difference being that this problem is more relevant for extragalactic astrophysical jets. The important difference is that now the ambient fluid has a density that is ten times larger than the jet density, i.e. $\rho_a = 10\gamma$. Because the density and pressure in the jet yield a sound speed of unity, the jet's velocity at the inlet is set to 100. These small changes makes the problem much more stringent, because the jet fluid is pushing an ambient fluid that is much denser than itself. The simulation was run to a time of 0.03. The problem was solved with a fourth order accurate ADER-WENO scheme using an HLL Riemann solver. (Though the code uses mechanisms to suppress the carbuncle instability in the linearized Riemann solver, it was not able to do that perfectly for this extreme problem.) A CFL number of 0.45 was used. The results from the final time are displayed.

Fig. 4a shows the log (base-10) color plot of the density. Fig. 4b shows the same for the pressure. Fig. 4c shows the magnitude of the velocity. The methods developed in this paper were applied to the simulation that is reported in Fig. 4. We see that the densities and pressures are positive and the jet's evolution is symmetrical, as expected. The jet's evolution is much slower and the working surface of the jet becomes susceptible to Rayleigh–Taylor instabilities. The cocoon of the jet also has a tendency to become Kelvin–Helmholtz unstable, though those instabilities are suppressed here because of the reduced dimensionality and the absence of any impressed perturbation. The working surface of the light jet generates very high pressures, and the high pressure fluid also propagates into the cocoon of the jet. Because the jet is light, it is very strongly compressed by the cocoon with the result that we can see a narrowing of the jet's channel in Fig. 4c as the jet propagates into the computational domain. The compression increases the jet's density with the result that after the first significant narrowing of the jet's channel the jet subsequently propagates as a heavy jet with a much smaller cross section. Most importantly, this small change in jet and ambient parameters makes this problem very applicable to extragalactic jets in astrophysics, all of which have large Mach numbers and jet densities that are initially ten to hundred times lower than the density of the ambient fluid.

This problem cannot be simulated when an unmodified second order TVD reconstruction is used along with a linearized or an HLL Riemann solver. Nor can it be simulated with unmodified higher order reconstruction when a simple density and pressure floor is provided to the Riemann solver. The methods developed here are crucial for a successful solution of this problem. We, therefore, offer the light jet problem as a more stringent variant of the problem discussed in Zhang and Shu [40].

3.3. 3D MHD blast problem with plasma beta of 1.005×10^{-3}

This is a three-dimensional variant on a two-dimensional problem that was first presented in Balsara and Spicer [4]. The plasma β measures the ratio of the thermal pressure to the magnetic pressure. As the plasma's β becomes smaller, this problem becomes increasingly stringent. The problem consists of a $\gamma = 1.4$ gas with unit density and a pressure of 0.1 initialized on a 129^3 zone mesh spanning the unit cube. Initially we have $B_x = B_y = B_z = 50/\sqrt{3}$. The pressure is reset to a value of 1000

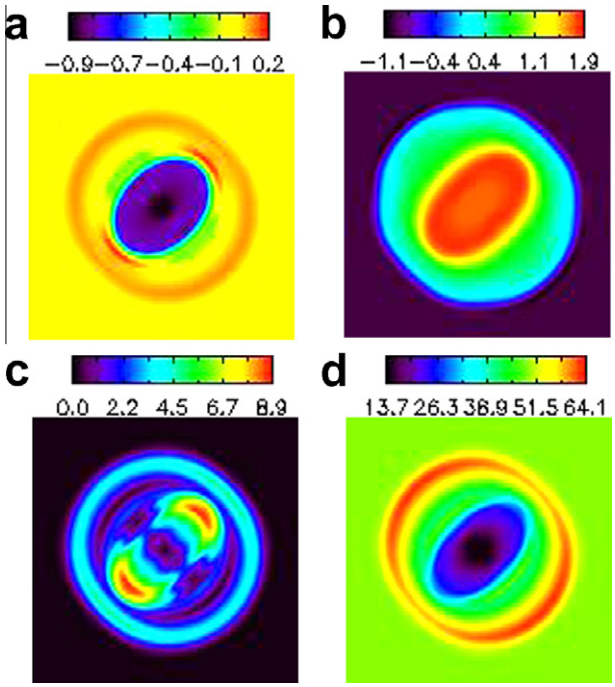

Fig. 5. a, b, c and d show the logarithmic density (base-10), logarithmic pressure (base-10), magnitude of the velocity and the magnitude of the magnetic field. The color bars show the logarithmic (base-10) values for the density and pressure and the magnitude of the velocity and magnetic field The range for the density (not log density) is [0.115, 2.53]; similarly, for the pressure, the range is [0.0135, 88.3]; for the magnitude of the velocity, the range is [0, 8.94] and for the magnitude of the magnetic field, the range is [13.7, 64.1].

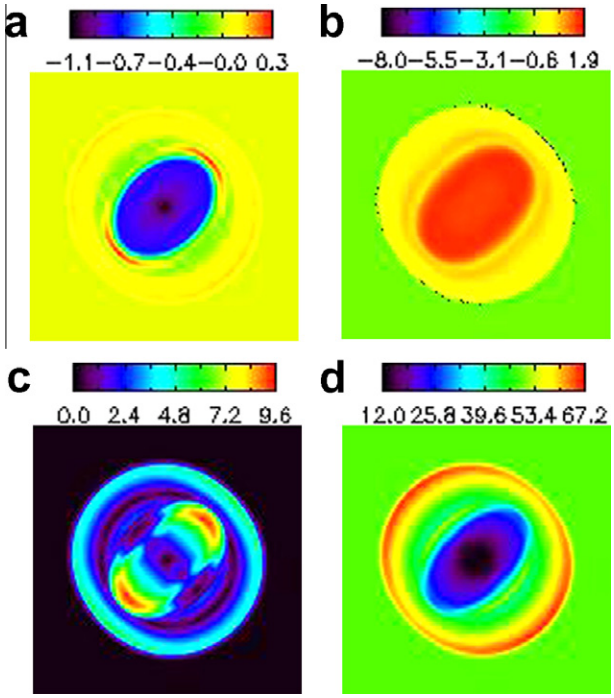

Fig. 6. a, b, c and d show the logarithmic density (base-10), logarithmic pressure (base-10), magnitude of the velocity and the magnitude of the magnetic field. In this simulation, the methods from this paper were not used. A linearized Riemann solver with floor values for the density and pressure was used instead. Notice the floor values for the pressure and the larger maximum values for the velocity and magnetic field. The color bars show the logarithmic (base-10) values for the density and pressure and the magnitude of the velocity and magnetic field The range for the density (not log density) is [0.08, 2.97]; similarly, for the pressure, the range is [10^{-}8, 87.94]; for the magnitude of the velocity, the range is [0, 9.6] and for the magnitude of the magnetic field, the range is [12.0, 67.2].

inside a central region with a radius of 0.1. The plasma's β is initially given by 1.005×10^{-3}. Such low values of β can indeed be reached in the sun's corona as well as in the magnetospheres of stars and planets. A CFL number of 0.3 was used. The problem is run up to a time of 0.012, by which time a strong magnetosonic blast wave propagates through the domain. The problem was run with a third order ADER-WENO scheme and a linearized Riemann solver. The use of a linearized Riemann solver instead of an HLL Riemann solver makes this problem more challenging.

Fig. 5a shows the log (base-10) color plot of the density for the mid-plane in the z-direction. Fig. 5b shows the same for the pressure in the same plane. Fig. 5c and d show the magnitude of the velocity and the magnitude of the magnetic field, again in the same plane. The methods developed in this paper were used in the simulation reported in Fig. 5. We see that the densities and pressures are positive as expected. The same problem can also be run successfully with second and fourth order ADER-WENO schemes.

We ran this problem over again with a simple density floor of 1×10^{-12} and a pressure floor of 1×10^{-8}. The same third order ADER-WENO scheme was used. This time around, we did not use the positivity preserving mechanisms that are presented in this paper. The log (base-10) density and pressure are shown in Fig. 6a and b. The velocity and magnetic field are shown in Fig. 6c and d. We see from Fig. 6b that the pressure variable is totally corrupted, to the point where it is scientifically unusable. We also see from Fig. 6a that the density variable is somewhat degraded and shows corrugations in response to the pressure variable. We further note that the maximum magnitudes of the velocity and magnetic field in Fig. 6c and d are larger, thus providing a physical explanation for the negative pressure. We hope, therefore, to have demonstrated the great utility of the methods presented here in astrophysical and space physics simulations.

4. Conclusions

We have presented a multidimensional, self-adjusting strategy for enforcing the positivity of density and pressure in hydrodynamic and MHD simulations. The method is based on examining the local flow to build a flattener variable, which identifies regions of strong shocks. The permitted range that the density and pressure can take is obtained in a self-adjusting fashion by scanning neighboring zones. Based on guidance provided by the flattener, the range is expanded in order to accommodate non-oscillatory reconstructions. Thus the clipping of extrema is avoided. We show that the density and pressure positivity enforcement can be obtained for MHD flows, in addition to Euler flows.

The method has been shown to work on very stringent problems for all orders up to fourth order of accuracy. The test problems used here have parameters that are quite similar to those that are attained in very difficult astrophysical and space physics problems. We used finite volume WENO reconstruction for all our test problems. The order of accuracy of the base level scheme is never degraded for smooth flow by the method presented here. While there are no barriers to extending it to even higher orders, drawing on the work of Balsara et al. [9] allows us to arrive at very efficient implementations of the scheme on structured meshes. The present method is easily extensible to DG schemes or unstructured meshes.

It is worth pointing out that all the schemes presented here relied on reconstruction that was carried out on the conserved variables. The more expensive characteristic limiting is avoided. As long as the simpler reconstruction is carried out in conjunction with the density and pressure positivity enforcing scheme described here, we have seen no need to resort to characteristic limiting. For that reason, the present paper seeks to elevate positivity to be a first ranked concept in the numerical solution of hyperbolic conservation laws, alongside with non-linear hybridization.

Acknowledgements

The author wishes to acknowledge support via NSF Grants NSF-AST-0947765 and NSF-AST-1009091. The author also acknowledges NASA Grants NASA-NNX07AG93G and NASA-NNX08AG69G. The majority of simulations were performed on a cluster at UND that is run by the Center for Research Computing.

Appendix A

To demonstrate how the velocity is brought within an acceptable range, let us focus on the x-velocity here. Using a formula that parodies Eq. (4) we can obtain $v_{x;i,j}^{\min-nbr}$ and $v_{x;i,j}^{\max-nbr}$. Since the velocities do not have to retain their sign, one can expand their range as follows:

$$v_{x;i,j}^{\min-extended} = v_{x;i,j}^{\min-nbr} - \kappa_2\left(v_{x;i,j}^{\max-nbr} - v_{x;i,j}^{\min-nbr}\right);\; v_{x;i,j}^{\max-extended} = v_{x;i,j}^{\max-nbr} + \kappa_2\left(v_{x;i,j}^{\max-nbr} - v_{x;i,j}^{\min-nbr}\right)$$

As before, we obtain $v_{x;i,j}^{q} \equiv v_{x;i,j}(x^q, y^q)$ at each of the nodal points within zone (i,j). For those zones where $v_{x;i,j}^{q}$ does not lie within the range $\left[v_{x;i,j}^{\min-extended}, v_{x;i,j}^{\max-extended}\right]$ we can reduce the variation using the same idea as before. Thus, say for example that $v_{x;i,j}^{q} < v_{x;i,j}^{\min-extended}$ for a particular node "q". We can then set

$$\tau_{i,j}^{q} = \frac{\bar{m}_{x;i,j} - \bar{\rho}_{i,j}\, v_{x;i,j}^{\min-extended}}{\bar{m}_{x;i,j} - \bar{\rho}_{i,j}\, v_{x;i,j}^{\min-extended} - m_{x;i,j}^{q} + \rho_{i,j}^{q}\, v_{x;i,j}^{\min-extended}}$$

The velocities are pulled back into the acceptable range by finding $\tau_{i,j} = \min\left(\tau_{i,j}^1, \tau_{i,j}^2, \ldots, \tau_{i,j}^Q,\right)$. As before, $\tau_{i,j}$ can now be used to shrink the spatially varying part of all the x-velocity variables in zone (i,j).

Next we demonstrate how the magnetic field is brought within an acceptable range. Let us focus on the x-magnetic field here. As with the velocities, we can obtain the range $\left[B_{x;i,j}^{\min-extended}, B_{x;i,j}^{\max-extended}\right]$. Also, as before, we can obtain $B_{x;i,j}^q \equiv B_{x;i,j}(x^q, y^q)$ at each of the nodal points within zone (i,j). Because the magnetic field is a conserved variable, just like the density, the process of bringing it within the acceptable range is much like that for the density. Thus, say for example that $B_{x;i,j}^q < B_{x;i,j}^{\min-extended}$ for a particular node "q". Recall, however, from Eq. (13) that some of the modes are needed for the consistency condition and their contribution at the node "q" is given by $\overline{\mathbf{B}}_{x;i,j}^q$. As long as $\overline{B}_{x;i,j}^q \geqslant B_{x;i,j}^{\min-extended}$, we can then set

$$\tau_{i,j}^q = \frac{B_{x;i,j}^{\min-extended} - \overline{\mathbf{B}}_{x;i,j}^q}{B_{x;i,j}^q}$$

As long as $B_{x;i,j}^{\min-extended} \leqslant \overline{B}_{x;i,j}^q \leqslant B_{x;i,j}^{\max-extended}$, the magnetic field can always be brought into the acceptable range using the same strategy as was used for the velocities. We also note that $B_{x;i,j}^{\min-extended} \leqslant \overline{B}_{x;i,j}^q \leqslant B_{x;i,j}^{\max-extended}$ can always be ensured at second order. Consequently, even for the worst of the worst situations one can always locally drop the order of accuracy to bring the magnetic field within bounds.

Appendix B. Supplementary data

Supplementary data associated with this article can be found, in the online version, at doi:10.1016/j.jcp.2012.01.032.

References

[1] R. Abgrall, Approximation du problème de Riemann vraiment multidimensionnel des èquations d'Euler par une methode de type Roe, I: La linèarisation, C. R. Acad. Sci. Ser. I 319 (1994) 499.
[2] R. Abgrall, Approximation du problème de Riemann vraiment multidimensionnel des èquations d'Euler par une methode de type Roe, II: Solution du probleme de Riemann approchè, C. R. Acad. Sci. Ser. I 319 (1994) 625.
[3] D.S. Balsara, D.S. Spicer, Maintaining pressure positivity in magnetohydrodynamic simulations, J. Comput. Phys. 148 (1999) 133–148.
[4] D.S. Balsara, D.S. Spicer, A staggered mesh algorithm using high order Godunov fluxes to ensure solenoidal magnetic fields in magnetohydrodynamic simulations, J. Comput. Phys. 149 (1999) 270–292.
[5] D.S. Balsara, C.-W. Shu, Monotonicity preserving weighted non-oscillatory schemes with increasingly high order of accuracy, J. Comput. Phys. 160 (2000) 405–452.
[6] D.S. Balsara, Second-order-accurate schemes for magnetohydrodynamics with divergence-free reconstruction, Astrophys. J. Suppl. 151 (2004) 149–184.
[7] D.S. Balsara, T. Rumpf, M. Dumbser, C.-D. Munz, Efficient, high-accuracy ADER-WENO schemes for hydrodynamics and divergence-free magnetohydrodynamics, J. Comput. Phys. 228 (2009) 2480.
[8] D.S. Balsara, Multidimensional extension of the HLL Riemann solver; application to Euler and magnetohydrodynamical flows, J. Comput. Phys. 229 (2010) 1970–1993.
[9] D.S. Balsara, M. Dumbser, C. Meyer, H. Du, Z. Xu, Efficient Implementation of ADER schemes for Euler and Magnetohydrodynamic flow on structured meshes – Comparison with Runge–Kutta methods, J. Comput. Phys. (submitted for publication).
[10] D.S. Balsara, A two-dimensional HLLC Riemann solver for conservation laws: Application to Euler and magnetohydrodynamic flows, submitted, J. Comput. Phys. (submitted for publication).
[11] T.J. Barth, P.O. Frederickson, Higher order solution of the Euler equations on unstructured grids using quadratic reconstruction, AIAA Paper no. 90-0013, 28th Aerospace Sciences Meeting, January (1990).
[12] T.J. Barth, Aspects of Unstructured Grids and Finite-Volume Solvers for Euler and Navier–Stokes Equations, VKI/NASA/AGARD Special Course on Unstructured Grid Methods for Advection Dominated Flows, AGARD Publ. R-787 (Von Karmen Institute for Fluid Dynamics, Belgium, 1995)
[13] B. Cockburn, C.-W. Shu, TVB Runge–Kutta local projection discontinuous Galerkin finite element method for conservation laws II: general framework, Math. Comput. 52 (1989) 411–435.
[14] B. Cockburn, C.-W. Shu, The Runge–Kutta discontinuous Galerkin method for conservation laws V, J. Comput. Phys. 141 (1998) 199–224.
[15] P. Colella, P. Woodward, The piecewise parabolic method (PPM) for gas-dynamical simulations, J. Comput. Phys. 54 (1984) 174–201.
[16] P. Colella, Multidimensional upwind methods for hyperbolic conservation laws, J. Comput. Phys. 87 (1990) 171.
[17] M. Dumbser, M. Käser, Arbitary high order non-oscillatory finite volume schemes on unstructured meshes for linear hyperbolic systems, J. Comput. Phys. 221 (2007) 693–723.
[18] M. Dumbser, D.S. Balsara, E.F. Toro, C.D. Munz, A unified framework for the construction of one-step finite volume and discontinuous Galerkin schemes on unstructured meshes, J. Comput. Phys. 227 (2008) 8209–8253.
[19] B. Einfeldt, C.-D. Munz, P.L. Roe, B. Sjogreen, On Godunov type methods near low densities, J. Comput. Phys. 92 (1991) 273–295.
[20] K.F. Gurski, An HLLC-type approximate Riemann solver for ideal magnetohydrodynamics, SIAM J. Sci. Comput. 25 (2004) 2165.
[21] Y. Ha, C.L. Gardner, A. Gelb, C.-W. Shu, Numerical simulation of high Mach number astrophysical jets with radiative cooling, J. Sci. Comput. 24 (1) (2005) 29–44.
[22] Y. Ha, C.L. Gardner, Positive scheme numerical simulation of high Mach number astrophysical jets, J. Sci. Comput. 34 (2008) 247–259.
[23] G.-S. Jiang, C.-W. Shu, Efficient implementation of weighted ENO schemes, J. Comput. Phys. 126 (1996) 202–228.
[24] R.J. LeVeque, Wave propagation algorithms for multidimensional hyperbolic systems, J. Comput. Phys. 131 (1997) 327.
[25] X.-D. Liu, S. Osher, T. Chan, Weighted essentially non-oscillatory schemes, J. Comput. Phys. 115 (1994) 200–212.
[26] T. Miyoshi, K. Kusano, A multi-state HLL approximate Riemann solver for ideal magnetohydrodynamics, J. Comput. Phys. 208 (2005) 315–344.
[27] B. Perthame, C.-W. Shu, On positivity preserving finite volume schemes for Euler equations, Numer. Math. 73 (1996) 119.
[28] R. Sanders, A third-order accurate variation nonexpansive difference for single non-linear conservation law, Math. Comput. 51 (1988) 535–558.
[29] C.-W. Shu, S.J. Osher, Efficient implementation of essentially non-oscillatory shock capturing schemes, J. Comput. Phys. 77 (1988) 439–471.
[30] C.-W. Shu, S.J. Osher, Efficient implementation of essentially non-oscillatory shock capturing schemes II, J. Comput. Phys. 83 (1989) 32–78.
[31] R.J. Spiteri, S.J. Ruuth, A new class of optimal high-order strong-stability-preserving time-stepping schemes, SIAM J. Numer. Anal. 40 (2002) 469–491.

[32] R.J. Spiteri, S.J. Ruuth, Non-linear evolution using optimal fourth-order strong-stability preserving Runge–Kutta methods, Math. Comput. Simulat. 62 (2003) 125–135.
[33] V.A. Titarev, E.F. Toro, ADER: arbitrary high order Godunov approach, J. Sci. Comput. 17 (1–4) (2002) 609–618.
[34] V.A. Titarev, E.F. Toro, Finite volume WENO schemes for three dimensional conservation laws, J. Comput. Phys. 201 (2004) 238–260.
[35] E.F. Toro, V.A. Titarev, Solution of the generalized Riemann problem for advection-reaction equations, Proc. Roy. Soc. Lond. A 458 (2002) 271–281.
[36] E.F. Toro, M. Spruce, W. Speares, Restoration of contact surface in the HLL Riemann solver, Shock Waves 4 (1994) 25–34.
[37] K. Waagan, A positive MUSCL-Hancock scheme for ideal magnetohydrodynamics, J. Comput. Phys. 228 (2009) 6809.
[38] Z. Xu, Y. Liu, C.-W. Shu, Hierarchical reconstruction for discontinuous Galerkin methods on unstructured grids with a WENO-type linear reconstruction and partial neighboring cells, J. Comput. Phys. 228 (2009) 2194.
[39] Z. Xu, Y. Liu, C.-W. Shu, Hierarchical reconstruction for spectral volume method on unstructured grids, J. Comput. Phys. 228 (2009) 5787.
[40] X. Zhang, C.-W. Shu, On positivity preserving high order discontinuous Galerkin schemes for compressible Euler equations on rectangular meshes, J. Comput. Phys. 229 (2010) 8918.